Author Manuscript

Author Manuscript

Author Manuscript

Author Manuscript

HHS Public Access

Author manuscript

Methods. Author manuscript; available in PMC 2019 April 01.

Published in final edited form as:

Methods. 2018 April 01; 138-139: 39–46. doi:10.1016/j.ymeth.2018.01.004.

Direct Detection of Carbon and Nitrogen Nuclei for High-Resolution Analysis of Intrinsically Disordered Proteins using NMR Spectroscopy

E. B. Gibbs[1] and **R. W. Kriwacki**[1,2,3,*]

[1]Department of Structural Biology, St. Jude Children's Research Hospital, Memphis, Tennessee, United States

[2]St. Jude Graduate School of Biomedical Sciences, Memphis, Tennessee, United States

[3]Department of Microbiology, Immunology and Biochemistry, University of Tennessee Health Sciences Center, Memphis, Tennessee, United States

Abstract

Nuclear magnetic resonance spectroscopy (NMR) is a powerful technique for characterizing the structural and dynamic properties of intrinsically disordered proteins and protein regions (IDPs & IDRs). However, the application of NMR to IDPs has been limited by poor chemical shift dispersion in two-dimensional (2D) ^{1}H-^{15}N heteronuclear correlation spectra. Among the various detection schemes available for heteronuclear correlation spectroscopy, ^{13}C direct-detection has become a mainstay for investigations of IDPs owing to the favorable chemical shift dispersion in 2D $^{13}C'$-^{15}N correlation spectra. Recent advances in cryoprobe technology have enhanced the sensitivity for direct detection of both ^{13}C and ^{15}N resonances at high magnetic field strengths, thus prompting the development of ^{15}N direct-detect experiments to complement established ^{13}C-detection experiments. However, the application of ^{15}N-detection has not been widely explored for IDPs. Here we compare ^{1}H, ^{13}C, and ^{15}N detection schemes for a variety of 2D heteronuclear correlation spectra and evaluate their performance on the basis of resolution, chemical shift dispersion, and sensitivity. We performed experiments with a variety of disordered systems ranging in size and complexity; from a small IDR (99 amino acids), to a large low complexity IDR (185 amino acids), and finally a ~73 kDa folded homopentameric protein that also contains disordered regions (133 amino acids/monomer). We conclude that, while requiring high sample concentration and long acquisition times, ^{15}N-detection often offers enhanced resolution over other detection schemes in studies of disordered protein regions with low complexity sequences.

*For correspondence: richard.kriwacki@stjude.org.

Conflict of interest

The authors declare no conflicts of interest.

Supplementary material

A supplemental document containing Figures S1–S12 and Tables S1–S3 is provided.

Publisher's Disclaimer: This is a PDF file of an unedited manuscript that has been accepted for publication. As a service to our customers we are providing this early version of the manuscript. The manuscript will undergo copyediting, typesetting, and review of the resulting proof before it is published in its final citable form. Please note that during the production process errors may be discovered which could affect the content, and all legal disclaimers that apply to the journal pertain.

Author Manuscript Author Manuscript Author Manuscript Author Manuscript

Graphical Abstract

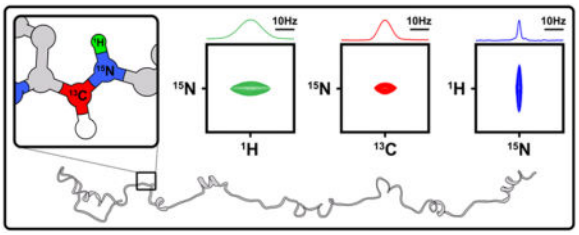

Keywords

Intrinsically disordered proteins; IDP; NMR; ^{13}C-Detection; ^{15}N-Detection

1. Introduction

NMR is a powerful technique for studies of the structural and dynamic properties of biomolecules with atomic resolution in solution. Of particular interest are NMR studies of intrinsically disordered proteins, and disordered protein regions (IDPs and IDRs), because, due to their dynamic features, x-ray crystallography is often not possible or relevant. However, the study of IDPs and IDRs is often limited by poor chemical shift dispersion in heteronuclear correlation spectra [1]. For IDPs and IDRs (in the following, we use the term IDPs to mean both IDPs and IDRs), the absence of highly populated secondary and tertiary structure, extensive dynamics and conformational averaging, and low amino acid sequence complexity, homogenize the chemical environments of amino acid residues, leading to limited chemical shift dispersion and severe resonance overlap. These resolution challenges become more pronounced as the length of the polypeptide increases, thus placing practical limitations on the size of IDPs/IDRs for which full backbone resonance assignments can be made using traditional, ^{1}H-detection-based, multi-dimensional protein NMR techniques.

The extensive conformational flexibility that underlies poor NMR spectral dispersion is, however, associated with favorable magnetization relaxation properties, which provides opportunities to achieve ultra-high spectral resolution for IDPs. The NMR linewidth, or full-width at half-height (Δ_{FWHH}), of the Lorentzian lineshape is an important factor affecting the resolution and the signal-to-noise (S/N) ratio of NMR spectra. The value of Δ_{FWHH} is proportional to the transverse relaxation rate R_2 ($\Delta_{FWHH} = 1/\pi T_2 = R_2/\pi$); however, additional factors contribute to observed resonance linewidths, including conformational exchange, magnetic field (B_0) inhomogeneity, sample heterogeneities, and temperature gradients. The latter sources of resonance broadening can be minimized by using modern NMR spectrometers and probes and through preparation of monodisperse protein samples; given this, the intrinsic relaxation properties of the detected nuclei strongly influence the resolution and sensitivity that can be achieved in NMR spectra. Among the spin ½ nuclei present in proteins, those with small values of the gyromagnetic ratio (γ; *e.g.,* ^{13}C and ^{15}N) exhibit intrinsically lower sensitivity, as given by the relation $S_0 \propto \gamma_e \gamma_d^{3/2}$, where γ_e and γ_d correspond to the γ values for the excitation and detection nuclei, respectively. However, this can be compensated by slower relaxation rates relative to those for ^{1}H nuclei due to

Author Manuscript Author Manuscript Author Manuscript Author Manuscript

reduced dipole-dipole relaxation associated with low-γ nuclei [2]. These properties were originally exploited in a series of *"proton-less"* ^{13}C direct-detection heteronuclear correlation experiments [3], which have subsequently been widely applied in studies of IDPs. In addition, however, direct detection of ^{15}N resonances for backbone amide groups ($^{15}N_H$) has re-emerged as a means to enhance resolution and sensitivity for systems that experience rapid amide group ^{1}H relaxation, including high molecular weight proteins [4]. However, the application of ^{15}N detection to IDPs has not been widely explored. To assess the benefits and limitations of ^{13}C and ^{15}N detection for IDPs, we analyzed $^{1}H_N$, $^{13}C'$, and $^{15}N_H$ resonance line shapes and compared detection schemes for the most commonly used 2D correlation experiments, including 2D ^{1}H-^{15}N and ^{13}C-^{15}N correlation experiments. As test cases, we investigated the central, Arf binding IDR of the E3 ubiquitin-protein ligase Hdm2 (Hdm2-ABD; residues 210 to 304) [5], a 182 amino acid, low complexity region of Surfeit locus protein 6 (Surf6-N; residues 1 to 182) [6], and a 130 amino acid region of Nucleophosmin (NPM1) that contains the pentamerization domain (residues 13–119) and two flanking IDRs (N130; residues 1 to 130) [7].

2. Materials and Methods

2.1. Protein Expression and purification

Hdm2-ABD—The Arf binding domain of Hdm2 (residues 210–304) with an N-terminal polyhistidine tag was expressed in *Escherichia coli* (*E. coli*) BL21 (λDE3) from the pET28a expression vector (Novagen) as described previously [5]. ^{13}C/^{15}N-labeled Hdm2-ABD was expressed using MOPS-based minimal media [8] containing [^{13}C] D-glucose and $^{15}NH_4Cl$ (Cambridge Isotope Laboratories). Cultured cells were harvested by centrifugation and lysed in 25 mM Tris HCl (pH 8.0), 500 mM NaCl, 5 mM β-mercaptoethanol (BME), and protease inhibitor cocktail (Sigma) by sonication. Lysates were clarified by centrifugation and Urea was added to the clarified extract to a concentration of 3 M. His-tagged Hdm2-ABD was purified by Ni^{2+}-NTA affinity chromatography and eluted with buffer containing 6 M urea and 0.5 M Imidazole. Fractions containing Hdm2-ABD were dialyzed against 25 mM Tris HCl (pH 8.0), 150 mM NaCl, 5 mM BME and treated with thrombin to cleave the His tag. Cleaved Hdm2-ABD was buffer exchanged by dialysis into 25 mM sodium phosphate (pH 7.0), 50 mM NaCl and further purified using anion-exchange chromatography (Q Sepharose; Amersham Pharmacia Biotech, Inc.) using a linear gradient of 0.05′1 M NaCl over 0.1 L. NMR experiments were performed at a protein concentration of 1 mM in 25 mM Sodium Phosphate pH 6.0, 10 mM NaCl, 0.03 % NaN_3, and 10% D_2O.

Surf6-N—Surf6-N (residues 1–182 of human Surf6) was cloned into a pET28a expression vector encoding an N-terminal polyhistidine tag and a tobacco etch virus protease (TEV) cleavage site. *E. coli* Rosetta2 (DE3) cells were grown at 37 °C in MOPS based minimal media containing [^{13}C] D-glucose and $^{15}NH_4Cl$ (Cambridge Isotope Laboratories) to an optical density at 600 nm of 1.0 and expression was induced by the addition of 0.4 mM Isopropyl β-D-1-thiogalactopyranoside (IPTG) followed by incubation at 37 °C for an additional 3 hours. Cultured cells were harvested by centrifugation. Surf6-N was purified from inclusion bodies using the following procedure. Cells were lysed in 25 mM Tris HCl (pH 8.0), 500 mM NaCl, 5 mM β-mercaptoethanol (BME), 0.1% Triton-1000, and protease

Author Manuscript Author Manuscript Author Manuscript Author Manuscript

inhibitor cocktail (Sigma). The crude lysates were clarified by centrifugation and the supernatant was removed. The insoluble fraction was resuspended in buffer containing 8M GuHCl and disrupted by sonication. Following an additional round of centrifugation, Surf6-N was purified by Ni^{2+}-NTA affinity chromatography and eluted with buffer containing 6 M urea and 0.5 M Imidazole. Fractions containing Surf6-N were dialyzed against 25 mM Tris HCl (pH 8.0), 500 mM NaCl, 5 mM BME to remove the urea and treated with TEV protease to cleave the His tag. Cleaved Surf6-N was mixed with 6M urea buffer and passed over Ni^{2+} resin to remove the His tag and TEV protease. The column flow-through fraction was then concentrated by ultracentrifugation using a 10 kDa MWCO filter (Amicron) and further purified by HPLC using an H_2O/CH_3CN/0.1% trifluoroacetic acid solvent system. NMR experiments were performed at a protein concentration of 1 mM in 25 mM Sodium Phosphate pH 7.0, 500 mM NaCl, 5 mM DTT, 0.03 % NaN_3, and 10% D_2O.

N130—N130 (human NPM1 residues 1–130) was expressed in *E. coli* as described previously [7]. N130 was purified via Ni^{2+}-NTA affinity chromatography, followed by proteolytic removal of the polyhistidine tag by TEV protease followed by HPLC using an H_2O/CH_3CN/0.1% trifluoroacetic acid solvent system. NMR experiments were performed at a protein concentration of 400 μM in 10 mM Tris HCl pH 7.0, 150 mM NaCl, 2 mM DTT, 0.03 % NaN_3, and 10% D_2O.

NMR Spectroscopy—All experiments were collected at 298 K on a Bruker AVANCE NEO spectrometer operating at a proton frequency of 800 MHz equipped with a TXO cryoprobe optimized for ^{13}C. For 1D spectra, processing (including Fourier transform and phase correction) and peak integration was performed by global spectral deconvolution using MestReNova software (Mestrelab Research). 2D Spectra were acquired with acquisition times corresponding to >3 X T_2 and >1 X T_2 in the F_2 and F_1 dimensions, respectively. 2D spectra were processed using data points corresponding to 3.14 X T_2 and 1 X T_2 in the F_2 and F_1 dimensions, respectively, and each dimension was zero-filled to the next power of 2. Apodization was performed by applying a cosine function (Shifted-Sine Bell; SSB = 2) and forward linear prediction was applied to complex data using 32 coefficients. 2D spectra were processed in Topspin 4.0 (Bruker). For 2D spectra, peak picking and integration by Gaussian fitting was performed using the program Sparky (UCSF).

3. Results

3.1. Choosing the Optimal Nucleus for Direct Detection; Analysis of Lineshapes in 1D NMR spectra for a Prototypical IDR, Hdm2-ABD

Backbone atoms in IDPs generally experience rapid local motions (*e.g.,* local correlation times of <6 ns] [9]) that are uncorrelated with those in distal protein regions, giving rise to large transverse relaxation times (T_2 values) and sharp resonances. This is exemplified in 1D spectra for $^{13}C/^{15}N$–labeled Hdm2-ABD; for example, ΔV_{FWHH} values for ^1H_N resonances were 4.7 ± 0.6 Hz (Fig. 1A, Fig. S1, Table S1), those for $^{13}C'$ resonances were 5.4 ± 1.5 Hz (Fig. 1B, Fig. S2, Table S1), and, finally, those for $^{15}N_H$ resonances were 1.2 ± 0.3 Hz (Fig. 1C, Fig. S3, Table S1), by far the sharpest. The Δv_{FWHH} values are consistent with

Author Manuscript Author Manuscript Author Manuscript Author Manuscript

theoretical predictions for $^{1}H_{N}$, $^{13}C'$, and $^{15}N_{H}$ transverse relaxation rates for these nuclei in a uniformly $^{13}C/^{15}N$-labelled protein at 800 MHz [2] and highlight the potential of ^{15}N-detection for yielding narrow linewidths and optimal spectral resolution for IDPs.

3.2. Choosing the Optimal Heteronuclear Correlation Scheme; Comparison of 2D Spectra for Disordered Proteins of Varying Size and Sequence Complexity

We next evaluated the resolution and sensitivity associated with different detection schemes for recording 2D ^{1}H-^{15}N and ^{13}C-^{15}N correlation spectra for several IDRs. These two types of 2D spectra were chosen for analysis here because they are the basis for commonly used multi-dimensional NMR experiments used for establishing backbone resonance assignments. For 2D ^{1}H-^{15}N correlation spectra, the ^{1}H-detected ^{1}H-^{15}N HSQC [10] (Fig. S4) and ^{15}N-detected ^{1}H-^{15}N INEPT (Fig. S5) experiments were used. For 2D ^{13}C-^{15}N correlation spectra, the ^{13}C-detected CON-IPAP experiment [3] (Fig. S6) and ^{15}N-detected CON experiment [11] (Fig. S7) were used.

The results for 2D ^{1}H-^{15}N correlation experiments with Hdm2-ABD, recorded for similar times (~5 hours for each) showed that most non-proline resonances (96 expected resonances) were resolved using either detection scheme, although the average S/N ratio for the ^{1}H-detected spectrum was >16-fold greater than for the ^{15}N-detected spectrum (Fig. 2A,C; Table 1). The poor spectral dispersion associated with IDPs, especially in the ^{1}H dimension of 2D ^{1}H-^{15}N correlation spectra, can limit spectral resolution. However, given the relatively narrow $^{15}N_{H}$ resonances for Hdm2-ABD (~1 Hz), spectral resolution for the ^{1}H-deteced spectrum was sufficient to resolve 88 out of 96 possible resonances. With the acquisition and apodization parameters used for the ^{1}H-detected 2D spectrum, the resonance linewidths were ~15 Hz in the ^{1}H dimension and ~6 Hz in the ^{15}N dimension. When directly detecting ^{15}N magnetization, 91 of the 96 possible resonances were resolved owing to the enhancement in $^{15}N_{H}$ linewidths, which were ~3 Hz using our standardized acquisition scheme. These results demonstrate that for small, well behaved IDRs like Hdm2-ABD, the majority of resonances may be resolved using 2D ^{1}H-^{15}N correlation experiments, with ^{15}N-detection offering superior resolution although with dramatically reduced sensitivity.

In contrast to Hdm2-ABD, Surf6-N is a 182 residue-long IDR that exhibits low sequence complexity and self-association that leads to broadening of some resonances. Consequently, the average Δ_{FWHH} values from 1D NMR lineshape analysis were larger than those measured for Hdm2-ABD, with values of 15.4 ± 1.8 Hz, 6.18 ± 1.2 Hz, and 3.4 ± 2.4 Hz for $^{1}H_{N}$, $^{13}C'$, and $^{15}N_{H}$ resonances, respectively (Fig. S8, Table S2). Note that, due to extensive resonance overlap, $^{1}H_{N}$ line widths were determined using a very high resolution 2D ^{1}H-^{15}N HSQC spectrum (Fig. S8 A,D). Furthermore, the ^{1}H-detected 2D ^{1}H-^{15}N HSQC spectrum (that used 3.14 X T_{2} data points in the ^{1}H dimension) exhibited extensive resonance overlap (Fig. 2B,D). Resonance linewidths were ~26 Hz in the $^{1}H_{N}$ dimension and ~10 Hz in the $^{15}N_{H}$ dimension, permitting resolution of 142 of the 177 possible resonances. Using ^{15}N-detection, the resonance linewidths were ~31 Hz in the $^{1}H_{N}$ dimension and ~7 Hz in the $^{15}N_{H}$ dimension, yielding an additional 13 well resolved resonances (Table 2). However, it should be noted that chemical shift perturbations were observed for several resonances as a result of sample heating (Fig. 2B, inset, Fig. S9),

Author Manuscript Author Manuscript Author Manuscript Author Manuscript

presumably due to the high decoupling pulse power applied during detection that was exacerbated by the high salt concentration in the sample buffer used (500 mM NaCl). This demonstrates that for a large IDR, spectral crowding can be partially overcome through the enhanced resolution provided by ^{15}N-detection. In this case, probably due to the high salt concentration [12] or the differential effects of transient self-association on $^{1}H_N$ and $^{15}N_H$ line widths, the signal-to-noise advantage of detecting ^{1}H was only ~6.5 (*versus* ~16 for the corresponding spectra for Hdm2-ABD) (Table 1). This example illustrates the potential of ^{15}N-detection to improve resolution in 2D^{1}H-^{15}N correlation spectra of challenging IDRs such as Surf6-N.

For IDPs, 2D ^{13}C-^{15}N correlation spectra provide enhanced chemical shift dispersion and tolerance to small variations in pH (in comparison with 2D ^{1}H-^{15}N correlation spectra) and, importantly, resonances for proline residues [13]. For Hdm2-ABD, 2D ^{13}C- ^{15}N correlation experiments recorded for similar times (~9 hours for each) show that almost all resonances were resolved using either detection scheme, although the average S/N ratio for the ^{13}C-detected spectrum was ~4-fold greater than that for the ^{15}N-detected spectrum (Fig. 2E,G). For the ^{13}C-detected spectrum, the average resonance linewidths were ~5 Hz in the ^{13}C' dimension and ~10 Hz in the $^{15}N_H$ dimension, yielding 96 of the 99 possible resonances. For the ^{15}N-detected spectrum, average resonance linewidths were ~3 Hz in the $^{15}N_H$ dimension and ~22 Hz in the indirect ^{13}C' dimension. Despite the limited resolution enforced by constant-time editing in the indirect ^{13}C dimension, the ^{15}N-detected ^{13}C-^{15}N correlation spectrum provided the largest number of resolved resonances (98 of 99).

For the ^{13}C-detected ^{13}C-^{15}N correlation spectrum for Surf6-N, the average resonance linewidths were ~8 Hz in the ^{13}C' dimension and ~10 Hz in the $^{15}N_H$ dimension, yielding 161 of the 185 possible resonances. For the ^{15}N-detected spectrum, average resonance linewidths were ~6 Hz in the $^{15}N_H$ dimension and ~21 Hz in the indirect ^{13}C' dimension, yielding 162 of 185 possible resonances. Furthermore, all the resonances that were observed in the ^{13}C-detect ^{13}C-^{15}N correlation spectrum were also observed in the ^{15}N-detected spectrum, with the exception of two resonances, presumably due to the lower sensitivity of ^{15}N detection. Therefore, in this case, where $^{15}N_H$ and ^{13}C' linewidths are more similar than with Hdm2-ABD, ^{15}N-detection provides only a slight resolution advantage and a less than 2-fold reduced S/N ratio (Table 2).

Taken together, our results show that for two IDRs that are characterized by rapid backbone conformational fluctuations and correspondingly slow transverse relaxation, $^{15}N_H$ linewidths were narrower than $^{1}H_N$ and $^{13}C'$, thus allowing ^{15}N-detection of 2D correlation spectra to afford the highest resolution at the expense of lower S/N. The S/N differential for ^{1}H- *versus* ^{15}N- detected 2D ^{1}H-^{15}N correlation spectra is much greater than for ^{13}C- *versus* ^{15}N-detected 2D ^{13}C-^{15}N correlation spectra. Therefore, ^{15}N-detection may be reserved for cases where the highest possible resolution in 2D ^{1}H-^{15}N correlation spectra is needed and the protein of interest can be prepared at high concentration (> 1 mM). In contrast, ^{15}N-detection may be optimally used to record 2D ^{13}C-^{15}N correlation spectra when $^{15}N_H$ line widths are significantly narrower than those for ^{13}C' nuclei, in which case the resolution advantages of ^{15}N-detection can be manifested. Estimates of ^{13}C' and $^{15}N_H$ line widths can be made from directly-detected 1D spectra and used to decide which detection strategy, ^{13}C

Author Manuscript Author Manuscript Author Manuscript Author Manuscript

versus ^{15}N, is likely to yield the highest resolution 2D ^{13}C-^{15}N correlation spectra. Based upon our results, we conclude that ^{15}N-detection should be considered for the analysis of IDPs that exhibit poor resonance dispersion due to large size and/or low sequence complexity.

3.3. Comparison of ^{1}H- and ^{15}N-detected TROSY-enhanced 2D ^{1}H-^{15}N Correlation Spectra for N130, a High Molecular Weight Folded Protein with Disordered Regions

The development of transverse relaxation-optimized spectroscopy (TROSY) [14] dramatically extended the size limits of detection of 2D ^{1}H-^{15}N correlation spectra for large molecular weight proteins. Additionally, the BEST-TROSY strategy that affords improved sensitivity and resolution was exploited in a set of multi-dimensional experiments to obtain sequential assignments for large IDPs [15]. Historically, TROSY has been utilized for ^{1}H-detection experiments; however, the long T_2 values of $^{15}N_H$ resonances have prompted the recent development of ^{15}N-detected TROSY experiments [4, 12]. Therefore, we tested ^{1}H- and ^{15}N-detection to record TROSY-enhanced 2D ^{1}H-^{15}N correlation spectra (Fig. S10 and S11, respectively) for the N-terminal oligomerization domain of Nucleophosmin (NPM1; termed N130), a 73.4 kDa homopentamer (residues 13–119, with a T_c value of 53.6 ± 0.9 ns) which also has two short IDRs (residues 1–13 and 120–130, with T_c values of 2.10 ± 0.05 ns for the latter segment) [16]. The first increments of ^{1}H- and ^{15}N-detected ^{1}H-^{15}N TROSY-enhanced correlation spectra were analyzed to estimate the T_2 values of resonances in the pentamerization domain (Fig. S12, Table S3); the average Δ_{FWHH} values of TROSY-enhanced $^{1}H_N$ and $^{15}N_H$ resonances were 22.7 ± 7.0 Hz and 7.6 ± 0.8 Hz, respectively. These values were used to establish acquisition parameters for the two 2D spectra according to our standard scheme (see Methods). For the ^{1}H-detected TROSY-enhanced 2D ^{1}H-^{15}N correlation spectrum, the average resonance linewidths were ~38 Hz and ~23 Hz in the $^{1}H_N$ and $^{15}N_H$ dimensions, respectively, for residues within the pentamerization domain and ~31 Hz and ~17 Hz, respectively for IDR residues (Fig. 3A,C; Table 3). The corresponding ^{15}N-detected 2D spectrum yielded slightly higher resolution albeit with lower sensitivity (~3-fold less). For example, the average resonance linewidths were ~43 Hz and ~15 Hz in the $^{1}H_N$ and $^{15}N_H$ dimensions, respectively, for residues within the pentamerization domain and ~39 Hz and ~12 Hz, respectively for IDR residues (Fig. 3B,D; Table 3). These results illustrate the benefits of ^{15}N detection for realizing the resonance narrowing effects of TROSY, especially for $^{15}N_H$ resonances of the large pentamerization domain. In addition, $^{15}N_H$ resonances for residues in the IDRs were narrower in the ^{15}N-detected 2D spectrum, illustrating the resolution advantage associated with ^{15}N detection for a large protein comprised of both a folded domain and IDRs.

4. Discussion

NMR studies of IDPs at atomic resolution are often challenging due to poor resonance dispersion, especially for backbone amide protons. Further, the general lack of secondary and tertiary structure leads to very similar chemical shift values for sidechain carbons of amino acids of the same type, often limiting the establishment of sequential resonance assignments. The latter factor is exacerbated by the low complexity that is associated with the sequences of many IDPs and IDRs. The advent of cryogenic NMR probes offering high-

Author Manuscript Author Manuscript Author Manuscript Author Manuscript

sensitivity detection of resonances for ^{13}C nuclei led to the development of a new generation of multi-dimensional NMR experiments based upon correlation of resonances for ^{13}C' and $^{15}N_H$ rather than ^{1}H and $^{15}N_H$ [3]. Because 2D ^{13}C-^{15}N correlation spectra offer improved spectral dispersion for IDPs, and because resonances of often abundant proline residues are detected, derivative multidimensional (≥3D) heteronuclear correlation experiments provided advantages for establishing sequential resonance assignments for IDPs [13, 17–20]. However, those based on sequential linkage of sidechain carbon resonances still suffered from amino acid-type chemical shift degeneracy, as discussed above. To overcome this problem, Showalter and co-workers developed a set of ^{13}C-deteted 3D heteronuclear correlation experiments that allowed resonance assignments to be established on the basis of the chemical shifts of sequential $^{15}N_H$ nuclei [13, 17]. However, the inclusion of two indirect ^{15}N dimensions in these experiments was non-ideal with regard to achieving the highest possible resolution due to the time demands of extensive sampling in the indirect ^{15}N dimensions. Recently, cryogenic NMR probes have become available that offer high sensitivity detection of $^{15}N_H$ resonances in addition to those of $^{13}C'$, offering the opportunity to explore the possible advantages of direct ^{15}N detection of spectra of IDPs and IDRs for improved resolution. Here, we compared spectral resolution and sensitivity for 2D ^{1}H-^{15}N and ^{13}C-^{15}N correlation spectra recorded through direct detection of each of the two correlated nuclei for two protein regions that are entirely disordered (Hdm2-ABD and Surf6-N) and 2D ^{1}H-^{15}N correlation spectra for a ~73 kDa folded, pentameric protein with two short IDRs (N130).

Our results for Hdm2-ABD showed that $^{15}N_H$ resonances were by far the narrowest (1.2 ± 0.3 Hz) amongst those also for $^{1}H_N$ and 13C′ nuclei (4.7 ± 0.6 Hz and 5.4 ± 1.5 Hz, respectively), and that this resolution advantage was manifested in improved resolution in ^{15}N-detected 2D ^{1}H-^{15}N (Fig. 2A,C) and ^{13}C-^{15}N correlation spectra (Fig. 2E,G). However, direct detection of ^{15}N resonances was accompanied by significantly reduced S/N ratios in comparison with the corresponding ^{1}H- and ^{13}C-detected 2D spectra. However, with a ~1 mM protein sample, the two ^{15}N-detected 2D correlation spectra were recorded in reasonable time periods (2D ^{1}H-^{15}N spectrum, ~4 ¾ hours; and ^{13}C- ^{15}N spectrum, 9 ¼ hours; Table 1). These measurement times were influenced by the design of our data sampling scheme, which involved linear sampling in the direct dimensions for >3 x T2 and in the indirect dimensions for >1 x T2 (except for the ^{15}N-detected 2D ^{13}C-^{15}N correlation experiment, which was limited by the need for a constant evolution time for the ^{13}C indirect dimension). This scheme was used to afford a level of resolution in both the directly and indirectly detected dimensions that was scaled to the relaxation properties of the relevant nuclei. This allowed for very high resolution in the directly detected dimensions and moderate resolution in the indirectly detected dimensions and also balanced considerations regarding sensitivity and total acquisition time.

Hdm2-ABD is a relatively small and well-behaved IDR and, despite its extensive disorder [21], yielded well resolved 2D ^{1}H-^{15}N and ^{13}C-^{15}N correlation spectra that did not provide the opportunity to illustrate the full potential of ^{15}N-detection for improved resolution. However, the Surf6-N IDR presented greater resolution challenges due to its larger size (185 *versus* 99 residues for Surf6-N and Hdm2-ABD, respectively), low sequence complexity (17.7% Ala, 15.5% Lys, 12.6% Glu and 11.0% Arg residues), and tendency for self-

Author Manuscript Author Manuscript Author Manuscript Author Manuscript

association (unpublished results, E. Gibbs and R. Kriwacki). In this case, ^{15}N-detection of the 2D ^{1}H-^{15}N correlation spectrum, which was recorded in ~3 hours, exhibited 155 resolved resonances *versus* 142 in the corresponding ^{1}H-detected spectrum (Fig. 2B, Table 1). In contrast, nearly identical numbers of resonances were resolved in the ^{13}C- and ^{15}N-detected 2D ^{13}C'-^{15}N correlation spectra for Surf6-N (161 and 162 resonances, respectively). This reflects the limitation on the maximal resolution that can be achieved in the ^{15}N-detected experiment used here due to constant time evolution in the indirect ^{13}C′ dimension (the Δ_{FWHH} value for ^{13}C′ was ~21 Hz in comparison with ~8 Hz in the ^{13}C-detected experiment; Table 1). Despite this limitation, these two spectra illustrate the advantage associated with 2D ^{13}C-^{15}N *versus* ^{1}H-^{15}N correlation spectra in resolving resonances for a challenging, moderately sized IDR.

We further evaluated the performance of ^{1}H- and ^{15}N-detection of 2D ^{1}H-^{15}N correlation spectra for N130, which is comprised of a highly stable, ~70 kDa pentamerization domain flanked by short N- and C-terminal IDRs [7]. As expected [2, 14], $^{15}N_H$ linewidths for resonances of residues in both the pentamerization domain and IDRs were much narrower than the corresponding $^{1}H_N$ resonances, and this was manifested in enhanced resolution in the ^{15}N-detected 2D spectrum. However, because N130 is a symmetric pentamer, it exhibits only 124 resonances for non-proline residues and does not present the degree of resonance overlap that would be associated with a single polypeptide chain protein comprised of a similar size folded domain and IDRs. In this latter case, ^{15}N-detection is likely to be required to achieve the highest possible spectral resolution in 2D ^{1}H-^{15}N correlation spectra, as discussed by Wagner and co-workers [2, 4].

In summary, recent technical developments enable direct detection of ^{1}H, ^{13}C, and ^{15}N nuclei for isotope-labeled disordered proteins in reasonable time periods given that high concentration (~1 mM) can be achieved. This allows optimization of data acquisition to address the poor spectral dispersion associated with NMR studies of IDPs. Our data for several IDRs shows that the $^{15}N_H$ resonance of amide groups is usually narrower than amide $^{1}H_N$ resonances and ^{13}C' resonances. Consequently, direct detection of $^{15}N_H$ resonances will afford 2D ^{1}H-^{15}N and ^{13}C-^{15}N correlation spectra with the highest possible resolution. However, this resolution advantage must be balanced against the sensitivity disadvantage associated with the low γ value of ^{15}N *versus* that for ^{1}H and ^{13}C. Because linewidths for $^{1}H_N$, ^{13}C', and $^{15}N_H$ resonances in IDPs can vary widely, we recommend assessing these linewidths for each protein and to choose a detection scheme accordingly. The amide $^{15}N_H$ resonance linewidth will usually be much narrower than the corresponding $^{1}H_N$ linewidth, favoring ^{15}N detection for high resolution when high protein concentration can be achieved. Alternatively, for proteins at lower concentrations (significantly less than 1 mM), ^{1}H detection of the 2D ^{1}H-^{15}N correlation spectrum with extended sampling in the indirect ^{15}N dimension may give the best compromise between resolution and sensitivity. In contrast to 2D ^{1}H-^{15}N correlation spectra, 2D ^{13}C-^{15}N correlation spectra allow detection of resonances for proline residues, and also afford improved spectral dispersion for IDPs due to the broader range of chemical shift values for ^{13}C' and $^{15}N_H$ resonances *versus* $^{15}H_N$ resonances. Our results showed that the linewidths of ^{13}C' resonances were 2-fold or less large than those for $^{15}N_H$ resonances, reducing the resolution benefits associated with direct ^{15}N detection. Nonetheless, direct ^{15}N detection was associated with slightly improved resolution in 2D

Author Manuscript Author Manuscript Author Manuscript Author Manuscript

^{13}C-^{15}N correlation spectra for Hdm2-ABD and Surf6-N (Tables 1 and 2) and these advantages may be more dramatically manifested in studies of larger IDPs displaying highly crowded 2D ^{13}C-^{15}N correlation spectra. In our experiments, we employed linear data sampling in the indirect dimensions of 2D correlation spectra and advocate optimizing this to match the relaxation behavior of the sampled nuclei. The use of non-uniform sampling in the indirect dimensions and data processing using other than Fourier transformation [22–24] are likely to further extend the resolution benefits of direct ^{15}N detection and also improve sensitivity, and should be utilized in the future. For ^{15}N-detected 2D ^{13}C-^{15}N correlation spectra, in particular, resolution enhancements may be afforded by using D_2O buffer [2] and greater sensitivity may be achieved using magnetization transfer pathways starting from H-alpha in analogy to ^{13}C-detected ^{13}C- ^{15} N correlation spectra described previously [18]. In conclusion, as had been demonstrated previously by others [3, 13], 2D ^{13}C-^{15}N correlation spectra afford superior spectral dispersion and resolution for IDPs and the advantages of this 2D fingerprint can be enhanced through ^{15}N detection when high protein concentration can be achieved.

Supplementary Material

Refer to Web version on PubMed Central for supplementary material.

Acknowledgments

The authors thank Mr. Cheon-Gil Park and Dr. Diana Mitrea for assistance with protein preparation; Drs. Grace Royappa, Youlin Xia, and Aaron Phillips for assistance with NMR spectroscopy; and Dr. Haribabu Arthanari (Harvard Medical School) for assistance with NMR spectroscopy and fruitful discussion. This work was supported by NIH R01CA092035 and 1R01GM115634 (to R.W.K.); National Cancer Institute Cancer Center Support Grant P30CA21765 (to SJCRH); and ALSAC (to SJCRH). E.G. is a recipient of an NIH Research Supplement to Promote Diversity in Health-related Research (R01GM115634-02S1).

References

1. Gibbs EB, Cook EC, Showalter SA. Application of NMR to studies of intrinsically disordered proteins. Arch Biochem Biophys. 2017; 628:57–70. [PubMed: 28502465]
2. Takeuchi K, Gal M, Shimada I, Wagner G. Low-gamma Nuclei Detection Experiments for Biomolecular NMR. Rsc Biomol Sci. 2012; 25:25–52.
3. Bermel W, Bertini I, Felli IC, Piccioli M, Pierattelli R. C-13-detected protonless NMR spectroscopy of proteins in solution. Prog Nucl Mag Res Sp. 2006; 48:25–45.
4. Takeuchi K, Arthanari H, Shimada I, Wagner G. Nitrogen detected TROSY at high field yields high resolution and sensitivity for protein NMR. J Biomol Nmr. 2015; 63:323–331. [PubMed: 26497830]
5. Bothner B, Lewis WS, DiGiammarino EL, Weber JD, Bothner SJ, Kriwacki RW. Defining the molecular basis of Arf and Hdm2 interactions. J Mol Biol. 2001; 314:263–277. [PubMed: 11718560]
6. Magoulas C, Zatsepina OV, Jordan PWH, Jordan EG, Fried M. The SURF-6 protein is a component of the nucleolar matrix and has a high binding capacity for nucleic acids in vitro. Eur J Cell Biol. 1998; 75:174–183. [PubMed: 9548374]
7. Mitrea DM, Grace CR, Buljan M, Yun MK, Pytel NJ, Satumba J, Nourse A, Park CG, Babu MM, White SW, Kriwacki RW. Structural polymorphism in the N-terminal oligomerization domain of NPM1. P Natl Acad Sci USA. 2014; 111:4466–4471.
8. Neidhardt FC, Bloch PL, Smith DF. Culture Medium for Enterobacteria. J Bacteriol. 1974; 119:736–747. [PubMed: 4604283]

Author Manuscript Author Manuscript Author Manuscript Author Manuscript

9. Jensen MR, Ruigrok RWH, Blackledge M. Describing intrinsically disordered proteins at atomic resolution by NMR. Curr Opin Struc Biol. 2013; 23:426–435.
10. Palmer AG, Cavanagh J, Wright PE, Rance M. Sensitivity Improvement in Proton-Detected 2-Dimensional Heteronuclear Correlation Nmr-Spectroscopy. J Magn Reson. 1991; 93:151–170.
11. Takeuchi K, Heffron G, Sun ZYJ, Frueh DP, Wagner G. Nitrogen-detected CAN and CON experiments as alternative experiments for main chain NMR resonance assignments. J Biomol Nmr. 2010; 47:271–282. [PubMed: 20556482]
12. Takeuchi K, Arthanari H, Imai MK, Wagner G, Shimada I. Nitrogen-detected TROSY yields comparable sensitivity to proton-detected TROSY for non-deuterated, large proteins under physiological salt conditions. J Biomol Nmr. 2016; 64:143–151. [PubMed: 26800993]
13. Bastidas M, Gibbs EB, Sahu D, Showalter SA. A primer for carbon-detected NMR applications to intrinsically disordered proteins in solution. Concept Magn Reson A. 2015; 44:54–66.
14. Pervushin K, Riek R, Wider G, Wuthrich K. Attenuated T-2 relaxation by mutual cancellation of dipole-dipole coupling and chemical shift anisotropy indicates an avenue to NMR structures of very large biological macromolecules in solution. P Natl Acad Sci USA. 1997; 94:12366–12371.
15. Solyom Z, Schwarten M, Geist L, Konrat R, Willbold D, Brutscher B. BEST-TROSY experiments for time-efficient sequential resonance assignment of large disordered proteins. J Biomol Nmr. 2013; 55:311–321. [PubMed: 23435576]
16. Mitrea DM, Cika JA, Guy CS, Ban D, Banerjee PR, Stanley CB, Nourse A, Deniz AA, Kriwacki RW. Nucleophosmin integrates within the nucleolus via multimodal interactions with proteins displaying R-rich linear motifs and rRNA. Elife. 2016; 5
17. Sahu D, Bastidas M, Showalter SA. Generating NMR chemical shift assignments of intrinsically disordered proteins using carbon-detected NMR methods. Anal Biochem. 2014; 449:17–25. [PubMed: 24333248]
18. Bermel W, Bertini I, Felli IC, Pierattelli R. Speeding Up C-13 Direct Detection Biomolecular NMR Spectroscopy. J Am Chem Soc. 2009; 131:15339–15345. [PubMed: 19795864]
19. Bermel W, Bertini I, Felli IC, Gonnelli L, Kozminski W, Piai A, Pierattelli R, Stanek J. Speeding up sequence specific assignment of IDPs. J Biomol Nmr. 2012; 53:293–301. [PubMed: 22684679]
20. Novacek J, Haba NY, Chill JH, Zidek L, Sklenar V. 4D Non-uniformly sampled HCBCACON and (1) J(NC alpha)-selective HCBCANCO experiments for the sequential assignment and chemical shift analysis of intrinsically disordered proteins. J Biomol Nmr. 2012; 53:139–148. [PubMed: 22580891]
21. Sivakolundu SG, Nourse A, Moshiach S, Bothner B, Ashley C, Satumba J, Lahti J, Kriwacki RW. Intrinsically Unstructured Domains of Arf and Hdm2 Form Bimolecular Oligomeric Structures In Vitro and In Vivo. J Mol Biol. 2008; 384:240–254. [PubMed: 18809412]
22. Novacek J, Zidek L, Sklenar V. Toward optimal-resolution NMR of intrinsically disordered proteins. J Magn Reson. 2014; 241:41–52. [PubMed: 24656079]
23. Mobli M, Hoch JC. Nonuniform sampling and non-Fourier signal processing methods in multidimensional NMR. Prog Nucl Mag Res Sp. 2014; 83:21–41.
24. Hyberts SG, Arthanari H, Robson SA, Wagner G. Perspectives in magnetic resonance: NMR in the post-FFT era. J Magn Reson. 2014; 241:60–73. [PubMed: 24656081]

Author Manuscript Author Manuscript Author Manuscript Author Manuscript

Highlights

- NMR detection schemes can be tailored to the unique linewidth features of IDPs.
- ^{15}N-detection often offers enhanced resolution over ^{1}H- or ^{13}C-detection schemes.
- High resolution ^{15}N-detection is balanced by intrinsically lower S/N.

Author Manuscript Author Manuscript Author Manuscript Author Manuscript

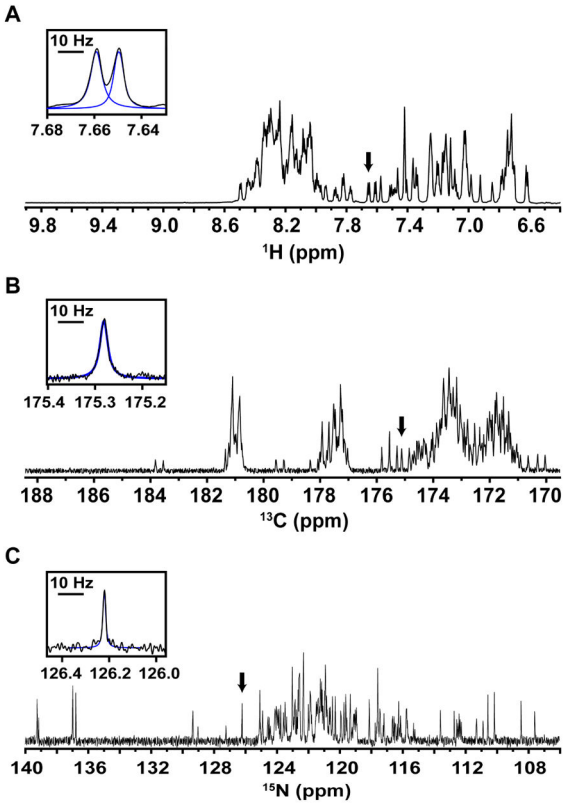

Figure 1.

1D NMR lineshape analysis for $^{13}C/^{15}N$ Hdm2-ABD. (A) The amide region of a 1D ^{1}H spectrum. (B) The carbonyl region of a 1D ^{13}C spectrum. (C) A 1D ^{15}N spectrum showing amide nitrogen resonances. Insets in each panel provide a detailed view of well resolved resonances, as indicated by the black arrows, along with the fits from global spectral deconvolution (blue; see Methods). The black bar corresponds to a width of 10 Hz. It should be noted that the carbonyl region was chosen here to assess the obtainable resolution of $^{13}C'$ direct detection. $^{13}C'$ linewidths are influenced by magnetic field strength due to chemical shift anisotropy and should not be used to generally assess all ^{13}C linewidths.

Author Manuscript Author Manuscript Author Manuscript Author Manuscript

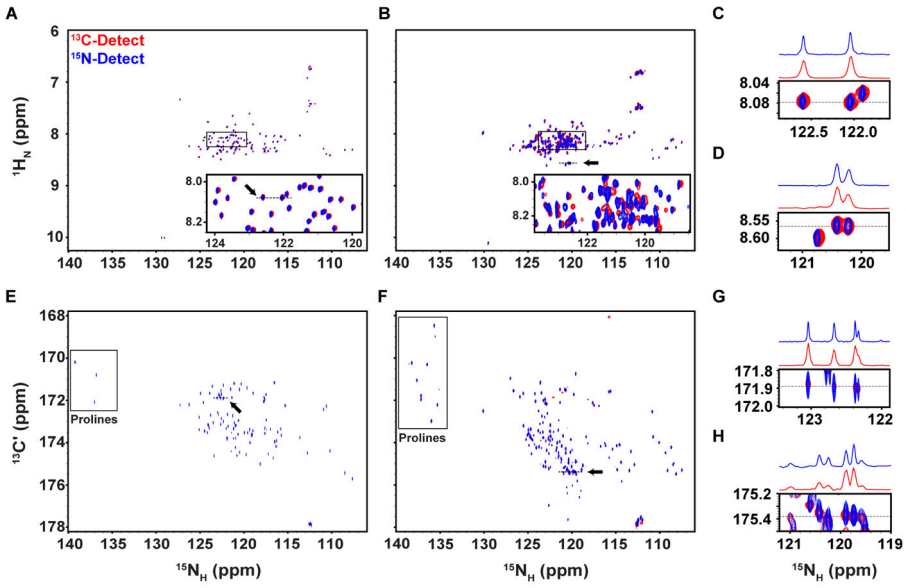

Figure 2.

Comparison of 2D heteronuclear correlation spectra for $^{13}C/^{15}N$ Hdm2-ABD and $^{13}C/^{15}N$ Surf6-N. (A) Overlaid ^{1}H- (red) and ^{15}N-detected (blue) 2D ^{1}H-^{15}N correlation spectra for Hdm2-ABD. The boxed region is shown enlarged with contours in the ^{1}H-detected spectrum scaled by 0.5 for clarity (A, inset) (B) Overlaid ^{1}H- (red) and ^{15}N-detected (blue) 2D ^{1}H-^{15}N correlation spectra for Surf6-N. The boxed region is shown enlarged with contours in the ^{1}H-detected spectrum scaled by 0.5 for clarity. Chemical shift perturbations were observed due to sample heating during decoupling (B, inset) (C) Zoomed view of a region from panel A, as indicated by the black arrow, with 1D projections along 8.08 ppm in the ^{1}H dimension (dotted line) highlighting the differences in ^{15}N linewidths. (D) Zoomed view of a region from panel B (black arrow), with 1D projections along 8.57 ppm in the ^{1}H dimension (dotted line) (E) Overlaid ^{13}C- (red) and ^{15}N-detected (blue) 2D $^{13}C'$-^{15}N correlation spectra for Hdm2-ABD. (F) Overlaid ^{13}C- (red) and ^{15}N-detected (blue) 2D $^{13}C'$-^{15}N correlation spectra for Surf6-N. In panels E and F, proline resonances are denoted by the boxed regions. (G) Zoomed view of a region from panel E (black arrow), with 1D projections along 171.9 ppm in the ^{13}C dimension (dotted line). (H) Zoomed view of a region from panel F (black arrow), with 1D projections along 175.4 ppm in the ^{13}C dimension (dotted line). Axes for ^{1}H and ^{13} C-detected spectra have been rotated for clarity.

Author Manuscript Author Manuscript Author Manuscript Author Manuscript

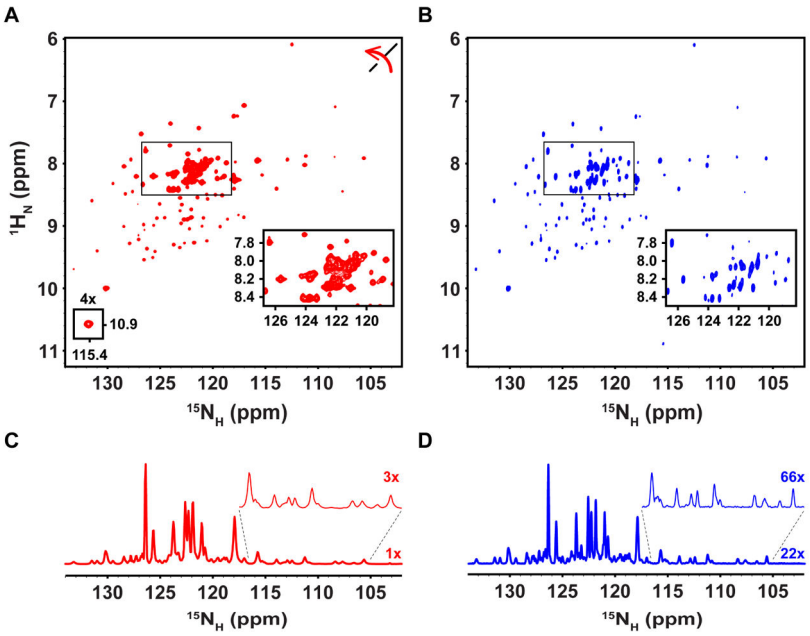

Figure 3.

Comparison of ^{1}H- and ^{15}N-detected TROSY-enhanced 2D ^{1}H-^{15}N correlation spectra for $^{2}H/^{15}N$ N130. (A) ^{1}H-detected TROSY-enhanced 2D ^{1}H-^{15}N correlation spectrum of N130, where the axes have been rotated for clarity. The small inset reveals a weak resonance (contoured at 4X). (B) ^{15}N-detected TROSY-enhanced 2D ^{1}H-^{15}N correlation spectrum of N130. The boxed regions in (A) and (B) are enlarged in the insets to show spectral regions containing resonances for IDR residues. (C) 1D projection in of ^{15}N dimension of the ^{1}H-detected spectrum in (A) showing $^{15}N_H$ linewidths. The expanded region of the spectrum, which contains pentamerization domain resonances, is scaled 3x for clarity. (D) 1D projection in the ^{15}N dimension of the ^{15}N-detected spectrum in (B) showing $^{15}N_H$ linewidths at a scale of 22x. The expanded region of the spectrum containing pentamerization domain resonances is shown at a scale of 66x for clarity.

Author Manuscript

Author Manuscript

Author Manuscript

Author Manuscript

Table 1

Acquisition parameters and observed spectral features for 2D heteronuclear correlation experiments performed on $^{13}C/^{15}N$ Hdm2-ABD.

Experiment	**$^{1}H,^{15}N$-HSQC**	**N_HNINEPT**	**^{13}C-CON**	**^{15}N-CON**
Points (F2 x F1)	4096 x 1500	5120 x 548	1024 x 1500	5120 x 136
Acquisition time (ms)	225 x 264	828 x 68	177 x 264	886 x 24
Scans	8	16	8	124
Recycle Delay (s)	1	1	1	1
Exp Time (hrs:min)	4:36	4:46	9:17	9:13
<FWHH $^{1}H_{N}$> (Hz)	15.1 ± 0.9 (n = 33)	15.3 ± 1.0 (n = 41)	--	--
<FWHH $^{13}C'$> (Hz)	--	--	4.9 ± 2.1 (n = 41)	21.7 ± 1.8 (n = 35)
<FWHH $^{15}N_{H}$> (Hz)	6.1 ± 1.3 (n = 33)	2.9 ± 1.1 (n = 41)	10.2 ± 1.0 (n = 41)	2.8 ± 0.8 (n = 35)
Signal-to-noise	3878	240	169	42
# peaks (observed/possible)	88/96	91/96	96/99	98/99

Author Manuscript

Author Manuscript

Author Manuscript

Author Manuscript

Table 2

Acquisition parameters and observed spectral features for 2D heteronuclear correlation experiments performed on $^{13}C/^{15}N$ Surf6-N.

Experiment	**$^{1}H,^{15}N$-HSQC**	**N_HNINEPT**	**^{13}C-CON**	**^{15}N-CON**
Points (F2 x F1)	2048 x 510	2048 x 154	1024 x 510	2048 x 104
Acquisition time (ms)	113 x 92	369 x 21	236 x 92	369 x 24
Scans	16	48	32	296
Recycle Delay (s)	1	1	1	1
Exp Time (hrs:min)	2:40	2:54	12:22	12:25
<FWHH $^{1}H_{N}$> (Hz)	26.1 ± 2.0 (n = 35)	30.7 ± 2.1 (n = 31)	--	--
<FWHH $^{13}C'$> (Hz)	--	--	7.5 ± 0.8 (n = 34)	20.9 ± 0.8 (n = 34)
<FWHH $^{15}N_{H}$> (Hz)	9.7 ± 1.5 (n = 35)	7.3 ± 1.6 (n = 31)	9.7 ± 1.5 (n = 34)	5.8 ± 1.0 (n = 34)
Signal-to-noise	923	143	142	80
# peaks (observed/possible)	142/177	155/177	161/185	162/185

Author Manuscript

Author Manuscript

Author Manuscript

Author Manuscript

Table 3

Acquisition parameters and observed spectral features for 2D heteronuclear correlation experiments performed on $^{2}H/^{15}N$ N130.

Experiment	**^{1}H-TROSY**	**^{15}N-TROSY**
Points (F2 x F1)	1024 x 218	1024 x 136
Acquisition time (ms)	45 x 42	198 x 14
Scans	64	96
Recycle Delay (s)	1	1
Exp Time (hrs:min)	4:18	4:31
<FWHH $^{1}H_{N}$> pentamer (Hz)	37.8 ± 3.2 (n = 20)	43.2 ± 3.9 (n = 20)
<FWHH $^{1}H_{N}$> IDR (Hz)	31.4 ± 1.9 (n = 8)	39.1 ± 2.2 (n = 8)
<FWHH $^{15}N_{H}$> pentamer (Hz)	22.9 ± 2.6 (n = 20)	15.2 ± 2.4 (n = 20)
<FWHH $^{15}N_{H}$> IDR (Hz)	17.4 ± 2.6 (n = 8)	11.6 ± 1.7 (n = 8)
Signal-to-noise	115	40
# peaks (observed/possible)	124/124	124/124